Journal of the Physical Society of Japan
Vol. 75, No. 5, May, 2006, 051010

Electronic Phases in an Organic Conductor α-(BEDT-TTF)$_2$I$_3$: Ultra Narrow Gap Semiconductor, Superconductor, Metal, and Charge-Ordered Insulator

Naoya TAJIMA*, Shigeharu SUGAWARA[1], Masafumi TAMURA, Yutaka NISHIO[1] and Koji KAJITA[1]

RIKEN, 2-1 Hirosawa, Wako, Saitama 351-0198
[1]*Department of Physics, Toho University, 2-2-1 Miyama, Funabashi, Chiba 274-8510*

(Received November 11, 2005; accepted December 12, 2005; published May 10, 2006)

We review the transport phenomena in an organic conductor α-(BEDT-TTF)$_2$I$_3$. It exhibits various types of transport depending on the circumstance in which it is placed. Under the ambient pressure, it is a charge-ordered insulator below 135 K. When high hydrostatic pressures are applied, it changes to a new type of narrow gap (or zero gap) semiconductor. The conductivity of this system is nearly constant between 300 and 1.5 K. In the same region, however, both the carrier (hole) density and the mobility change by about six orders of magnitude, in a manner so that the effects just cancel out giving rise to the temperature independent conductivity. The temperature (T) dependence of the carrier density n obey $n \propto T^2$ below 50 K. When it is compressed along the crystallographic a-axis, it changes from the charge ordered insulator to a narrow gap semiconductor. At the boundary between these phases, there appears a superconducting phase. On the other hand, when compressed in the b-axis, the system changes to a metal with a large Fermi surface. The effect of magnetic fields on samples in the narrow gap semiconductor phase was examined. Photo-induced transition from the charge ordered insulating state to a metallic state is also discussed.

KEYWORDS: α-(BEDT-TTF)$_2$I$_3$, transport phenomenon, ultra narrow gap semiconductor, hydrostatic pressure, uniaxial compression, photo-induced insulator–metal transition
DOI: 10.1143/JPSJ.75.051010

1. Introduction

For many years, organic conductors have been fascinating physicists as the basic materials for searching new physics. Rich variety of the electronic conductors; ranging from insulators to superconductors,[1)] and from one-dimensional to three-dimensional systems are found. Since organic materials are soft, they are sensitive to the pressure, and we can control the transport properties of electrons by applying the pressures.[2–5)] Application of strong electric fields,[6,7)] or magnetic field,[8–10)] and shedding light,[11,12)] are also effective to change the transport phenomena of organic conductors.

In this paper, we describe transport phenomena which the organic conductor α-(BEDT-TTF)$_2$I$_3$ shows when placed under high hydrostatic pressures,[13,14)] or it is uniaxially compressed.[3,15)] The effect of the magnetic field[16–19)] is also mentioned. Another issue discussed in this paper is the photoconduction phenomenon of this material in the charge ordered insulating state.[20)] Photo-induced insulator–metal transition was observed when a strong Laser pulse was incident on the sample.

The organic conductor α-(BEDT-TTF)$_2$I$_3$ is a member of the (BEDT-TTF)$_2$I$_3$ family.[21)] All the crystals in this family consist of conductive layers of BEDT-TTF molecules and insulating layers of I_3^- anions as shown in Fig. 1.[21–24)] The difference among them lies in the arrangement and orientation of BEDT-TTF molecules within the conducting plane and this difference gives rise to variations in the transport phenomena. Most of the members of this family are two-dimensional metals with large Fermi surfaces and some of them are superconducting with T_c values of several Kelvin.[22–24)] On the other hand, α-(BEDT-TTF)$_2$I$_3$ is different from other crystals. According to the band calculation,[25)] this system is a semimetal with two small Fermi surfaces; one with electron character and another with hole character (Fig. 2).

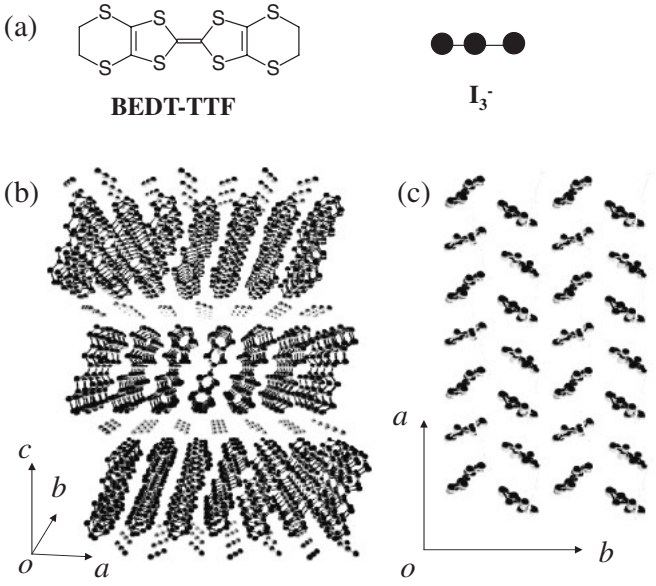

Fig. 1. (a) BEDT-TTF molecule and I_3^- molecule. (b) Crystal structure of α-(BEDT-TTF)$_2$I$_3$ viewed from b-axis. (c) Crystal structure viewed from c-axis.

When cooled, it behaves as a metal above 135 K where it undergoes a phase transition to an insulator as shown in

*E-mail: taji@riken.jp

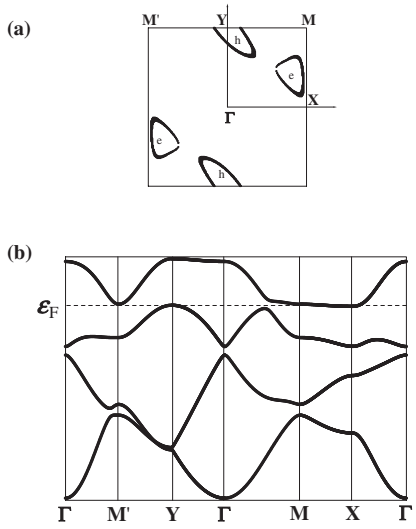

Fig. 2. (a) Fermi surface and (b) Band structure at room temperature. The position of the Fermi energy (ϵ_F) is indicated by a broken line.

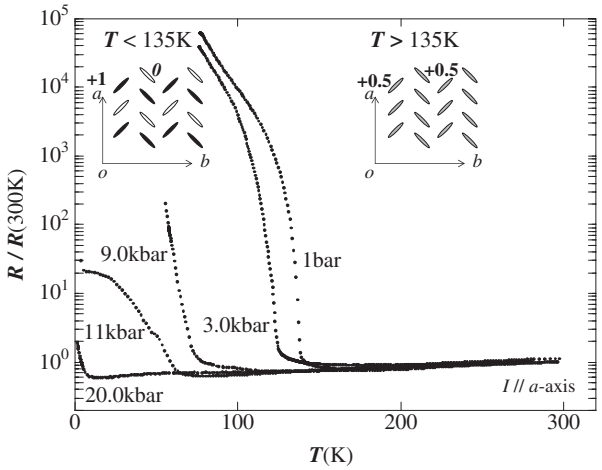

Fig. 3. Temperature dependence of the resistance under several hydrostatic pressures. The inset shows a schematic picture of the arrangement of BEDT-TTF molecules in a conducting layer viewed from the *c*-crystal axis and the charge pattern under the ambient pressure. At low temperatures below 135 K, horizontal charge stripes pattern for $+1e$ and 0 is formed.

Fig. 3.[21] In the insulator phase below 135 K, rapid decrease in the magnetic suscepibility indicates that the system is in a nonmagentic state with a spin gap.[26] According to the theoretical work by Kino and Fukuyama[27] and Seo[28] and the experimental investigation by Takano *et al.* (NMR)[29] and Wojciechowski *et al.* (Raman),[30] this transition is due to the charge disproportionation. At low temperatures below 135 K, horizontal charge stripes pattern for $+1e$ and 0 has been formed as shown in the inset of Fig. 3.

The effect of high hydrostatic pressure on the transport was first examined by Kartsovnik *et al.*[31] and Schwenk *et al.*[32] They found that under high pressures, the metal–insulator transition is suppressed and the system shows metallic behavior to the lowest temperature. This change in the electronic state accompanies the disappearance of the charge ordering as shown by the recent Raman experiment.[30] Application of uniaxial stress is also effective to suppress the transition.[3,5] Compression of the sample both in the *a*- and *b*-crystal axes suppress the transition.

2. α-(BEDT-TTF)$_2$I$_3$ under High Hydrostatic Pressures: Temperature Independent Conductivity

One of the characteristic features of the electric transport in this material is that the conductivity is nearly constant in the metallic region above 135 K as shown in Fig. 3. Placed under high hydrostatic pressures above 15 kbar, the metal–insulator transition is suppressed and the metallic region expands towards low temperatures (Fig. 3).[13,14,16,17]

This metallic state is peculiar. The conductivity is almost constant from 300 to 1.5 K. Usually, this implies that the sample is so dirty that impurity scattering dominates the conduction. However, the low temperature transport phenomena were found to be extremely sensitive to the magnetic field.[16,17] It contradicts the picture that the sample is dirty. To clarify the properties of carriers in this system in more detail, the Hall effect measurement is inevitable.

2.1 Strong temperature dependence of the carrier density and the mobility

The Hall effect in this system was first examined by Mishima *et al.* and they discovered strong temperature dependence of the Hall coefficient.[13] However, the magnetic field of 5 T they used was too high to investigate the electron properties in the zero field limit. It is because the electron system at low temperature is sensitive to the magnetic field and varies its character even in weak magnetic fields below 1 T. So, Tajima *et al.* reexamined the Hall effect using much lower magnetic fields.[14] Figure 4 gives the temperature dependence of the Hall coefficient for $B = 0.01$ T. The Hall coefficient was found to be positive in the whole range of temperature indicating the dominant carriers are holes. The most important finding is the strong temperature dependence of the Hall coefficient. It changes by about six orders of magnitude from 10^{-2} cm^3/C at 300 K to 10^4 cm^3/C at 1.5 K.[14]

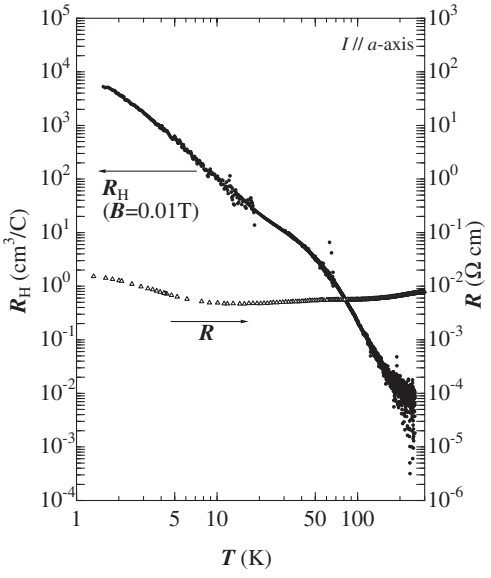

Fig. 4. Temperature dependence of the Hall coefficient and the resistance for $p = 18$ kbar.

This is the first material in which such a strong temperature dependence of the Hall coefficient is observed and yet, the conductivity remains constant in the wide temperature region. In this respect, α-(BEDT-TTF)$_2$I$_3$ under high pressures is a new type of conductor.

For a single carrier system with an isotropic energy band, the analysis of the data can go further as follows. From the Hall coefficient R_H, the carrier density n is determined as $n = 1/R_H e$. Then, the carrier mobility μ is calculated by combining n with the conductivity σ ($\mu = \sigma R_H$).

In the present case, however, the situation is somewhat complicated because this material is expected to be a semimetal (Fig. 2). For a semimetal, in which equal number of holes and electrons exist, the Hall coefficient is written as $R_H = (\mu_h - \mu_e)/(\mu_h + \mu_e)ne$ in terms of the mobility of holes μ_h and electrons μ_e and the carrier density $n = n_e = n_h$. In this situation, the Hall coefficient does not give the exact value of the carrier density. As a result, the mobility of electrons and holes also cannot be determined only from the R_H data.

In order to determine the carrier density and the mobility of holes and electrons in two carrier system, we need additional information. It is the magnetoresistance. The magnetoresistance M is defined as $M = \Delta\rho_0/\rho_0 = (\rho(B) - \rho_0)/\rho_0$. In low magnetic fields, the magnetoresistance M is proportional to the square of the magnetic field B as $M = (\mu_M B)^2$. Here, the parameter μ_M is called the magnetoresistance mobility.

Getting the value of μ_M is the first step. Then, the effective carrier density n_{eff} is calculated using the Hall coefficient as $R_H = 1/n_{eff}e$. Lastly, the effective mobility μ_{eff} is determined using the relation $\rho = 1/(n_{eff}e\mu_{eff})$.

The mobilities of holes and electrons can be separately determined using the effective mobility μ_{eff} and magneoresistance mobility μ_M. In the most simple two carrier system, the effective mobility and the magnetoresistance mobility are expressed as $\mu_{eff} = \mu_h - \mu_e$ and $\mu_M^2 = \mu_h \cdot \mu_e$. Putting the values of μ_{eff} and μ_M experimentally obtained, one can determine μ_h and μ_e.

Temperature dependence of the effective carrier density, effective mobility and magnetoresistance mobility are plotted in Fig. 5 in the range from 77 to 2 K.[33] We see μ_{eff} and μ_M are nearly equal in this temperature region. In this case ($\mu_{eff} = \mu_M$), the mobility of holes and electrons is estimated to be about 1.6 μ_{eff} and 0.6 μ_{eff}, respectively. On the other hand, the carrier density of holes and electrons are about 0.45 n_{eff}. These results indicate the value of the mobility of holes calculated based on the single carrier picture agree with that estimated based on the two carrier picture[33] within a factor of 2. In the following discussions, we assumed $\mu_h = \mu_{eff}$ and $n = n_{eff}$. Therefore, note that they include the ambiguity of factor of 2.

Returning to Fig. 5, we see both of the carrier density and the mobility of α-(BEDT-TTF)$_2$I$_3$ under high pressures depends strongly on temperature. They change by about six orders of magnitude from 300 to 1.5 K. An extremely high mobility about 3×10^5 cm^2/(V·s). is attained at low temperatures. The carrier density, on the other hand, decreases down to about 10^{15} cm^{-3} at the lowest temperature.

An experiment was done by Tajima *et al.* which intends to confirm the picture that carriers with high mobility contribute the transport phenomena at low temperatures. In the experiment, warping of the current path in the sample which is caused by the magnetic field is detected.

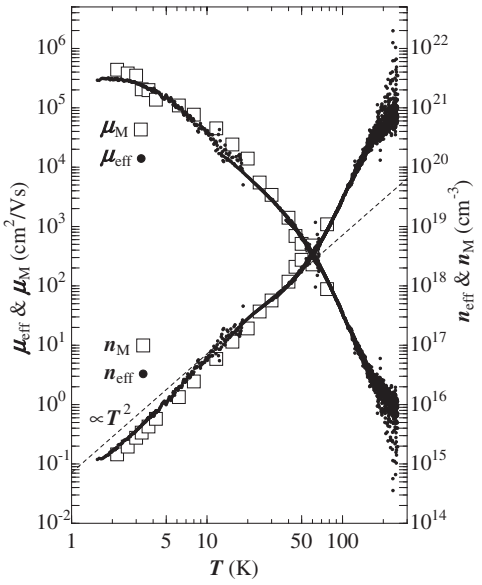

Fig. 5. Temperature dependence of the carrier density and the mobility for $p = 18$ kbar. The data plotted by ● is the effective carrier density n_{eff} and the mobility μ_{eff}. The magnetoresistance mobility μ_M and the density n_M, on the other hand, is shown by □ from 77 to 2 K. The results of two experiments agree well and the density obeys $n \propto T^2$ from 10 to 50 K (indicated by broken lines).

This effect of the warped current path in the magnetic field is often observed in semiconductors with high carrier mobility. In organic conductors, however, the experiment to detect this warping is not easy because of the difficulty in attaching many electrodes on a small and fragile sample. In the experiment described in ref. 14, eighteen-electrodes were attached to a sample with dimensions $2.2 \times 0.8 \times 0.05$ mm^3. Potential differences between various pairs of electrodes were measured as functions of magnetic fields. These data contain the information on the current path. First, the Hall angle was measured. Hall angle θ_H is defined as $\tan\theta_H = E_y/E_x$ in which E_x is the electric field component along the current direction and E_y is the Hall field. Experiments were done on a sample under the hydrostatic pressure of about 18 kbar at 4.2 K. The Hall angle θ_H at $B = +1$ T was about $+20^\circ$. Since the Hall angle depends linearly on the mobility of carriers and on the magnetic field, this large Hall angle evidences that holes with high mobility dominates the transport phenomenon. The carrier mobility was estimated to be about 4000 cm^2/(V·s) at 1 T. Secondly, warping of the current flow due to the strong effect of Lorentz force was examined in detail by detecting the potential difference between the electrodes. The experimental results were compared with the calculation which simulates the effect of the current path warping. The experimental results are well reproduced by the simulation assuming a carrier system with a high mobility. This experiment gives an evidence that the mobility of carries at low temperature is high.

At high temperatures, on the other hand, the carrier mobility is estimated to be about 1 cm^2/(V·s). This value is typical to many organic conductors at room temperatures. In

organic conductors at high temperatures, the effect of thermal agitation on the motion of carriers is so strong that the mobility is low.

In conclusion, it is established experimentally that α-(BEDT-TTF)$_2$I$_3$ under high pressures is truly a new type of conductor. In this system, the carrier mobility increases by about six orders from 300 to 1.5 K. This effect, however, is just cancelled out by the decrease in the carrier density, resulting in the resistance almost independent of temperature.

2.2 *Semiconducting state with an extremely narrow or a zero gap*

In this section, the electronic states of this system at low temperatures are discussed. As seen in Fig. 5, the carrier density decreases monotonically with decreasing temperature. From this behavior of the carrier density, this system is considered to be a semiconductor.

To get more information, the analysis of the data of temperature dependence of the carrier density was done introducing a few assumptions.[14] First, the Fermi energy dose not move with temperature. The second assumption is that the system is strictly two dimensional. Lastly, the carriers are assumed to be on a parabolic energy band with the mass isotropic in the two dimensional plane.

Based on these assumptions, the temperature dependence of the carrier density was calculated. The mass m^* and the band gap ε_g were chosen to give the best fit of carrier density in the temperature region below 3 K as shown in Fig. 6. The energy gap and effective mass of holes are estimated to be $\varepsilon_g < 1$ meV and $m^* \sim 0.02m_0$, where m_0 is the free electron mass.[14]

This energy gap should be compared with that in a typical narrow gap semiconductor $Cd_xHg_{1-x}Te$. For $x = 0.136$, it is about 10 meV.[34] The energy gap in the present system is narrower even than this value.

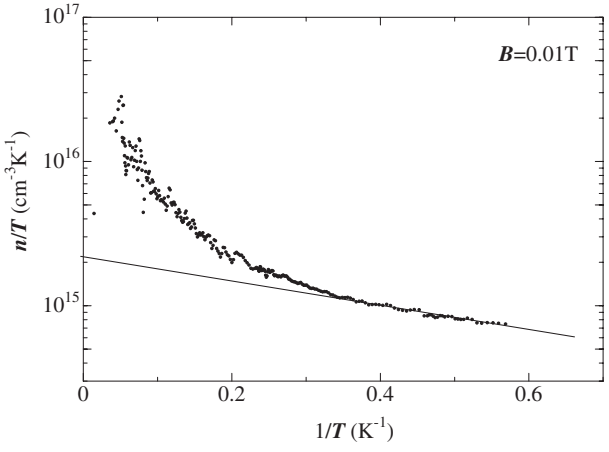

Fig. 6. An estimation of the energy gap ε_g and the effective mass m^*. The carrier density (n) in a two-dimensional semiconductor is expressed as $\ln(n(T)/T) = -\frac{\varepsilon_g}{2k_B}\frac{1}{T} + C$. Here, the constant C is written as $C = \ln(2k_BD) = \ln(2k_B\frac{m^*}{2\pi^2\hbar^2c})$, where D is the two-dimensional density of states and c is the lattice constant along the direction normal to the 2D-plane. The energy gap is estimated from the slope of the curve, and the effective mass is estimated from the intersection of the line at $1/T = 0$ which gives the value of C. Fitting the curve to the data at the lowest temperatures (below 3 K), we get $\varepsilon_g \simeq 1$ meV and $m^* \simeq 0.02m_0$.

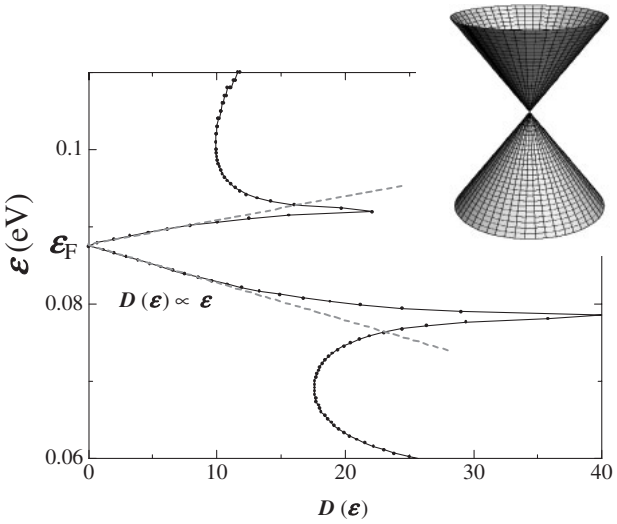

Fig. 7. The density of state and band structure (inset) near the Fermi level of α-(BEDT-TTF)$_2$I$_3$ under high pressure. In this calculation, we referred to the data of ref. 42.

These experimental results are, thus, interpreted assuming the system as an ultra narrow gap semiconductor. However the origin of the narrow gap structure was not clarified. Recently, Kobayashi *et al.* performed a band calculation for this material under high pressures and found the system to be a zero gap semiconductor (Fig. 7).[36] According to their calculation, the bottom of the conduction band and the top of the valence band contact at two points in the first Brillouin zone. In the vicinity of the contact points, carrier system has a Dirac cone type energy dispersion as shown in the inset of Fig. 7. Moreover, they found the zero gap structure of the energy band is stable against the change in the intermolecular transfer integrals of carriers. Standing on this picture, the experimental results was reexamined. If the system is a zero gap semiconductor, temperature dependence of the carrier density should obey not the exponential law but the power law. For two dimensional zero gap semiconductors, the carrier density is expected to depend on the temperature as $n = \int D(\varepsilon)f(\varepsilon)\,d\varepsilon \propto T^2$, where $D(\varepsilon)$ ($\propto \pm\varepsilon$ around the Fermi level) is the density of state as shown in Fig. 7 and the $f(\varepsilon)$ is the Fermi distribution function. Actually, the carrier density in Fig. 5 is proportional to T^2 in the region from 10 to 50 K.

Concluding this section, α-(BEDT-TTF)$_2$I$_3$ under high hydrostatic pressures is a new type of semiconductor with an extremely narrow gap less than 1 meV. Moreover, recent band calculations pointed out the possibility that it is a zero gap semiconductor with the Dirac cone type energy dispersion.

2.3 *Other organic narrow gap semiconductors*

Organic materials θ-(BEDT-TTF)$_2$I$_3$ under pressures $p >$ 5 kbar and α-(BEDT-TSF)$_2$I$_3$ ($p >$ 6 kbar) are ultra narrow gap semiconductors. They also have carrier systems with strongly temperature dependent density and mobility and their resistance is almost temperature independent. The temperature dependence of the carrier density and the mobility of the two crystals are shown in Fig. 8. Recently, a new narrow gap semiconductor α-(BEDT-STF)$_2$I$_3$ was

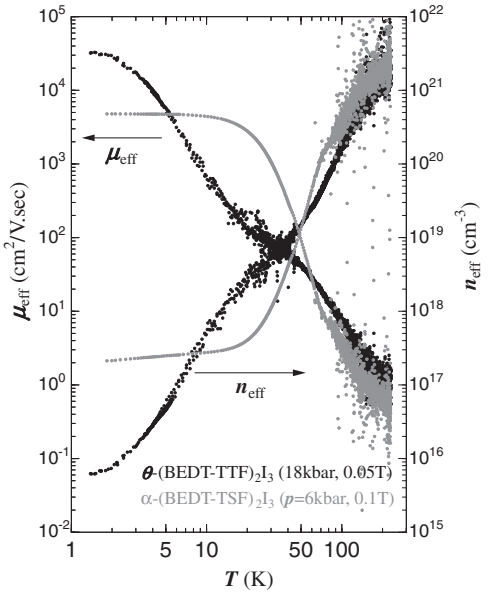

Fig. 8. The temperature dependences of the carrier densities and the mobilities of θ-(BEDT-TTF)$_2$I$_3$ under 18 kbar (black) and α-(BEDT-TSF)$_2$I$_3$ under 6 kbar (gray).

found. This material under the pressures above 18 kbar exhibits transport properties similar to the other organic narrow gap semiconductors.

2.3.1 θ-(BEDT-TTF)$_2$I$_3$

Under the ambient pressure, θ-(BEDT-TTF)$_2$I$_3$ is a typical two dimensional metal with large Fermi surfaces.[23,38–40] As the carrier mobility increases with decreasing temperature while the density is almost constant (10^{21} cm^{-3}) as shown in the inset of Fig. 10. The resistance drop by about two or three orders of magnitude occurs between 300 to 1.5 K.

Under the hydrostatic pressures above 5 kbar, on the other hand, this material changes to an ultra narrow gap semiconductor.[35] At the transition pressure, there appears a jump in the resistance.[35,40] It suggests that this transition is of the first order. The difference of the two phases appears in the temperature dependences of resistance. The low pressure phase is metallic; the resistance decreases with decreasing temperature. On the other hand, the sample in the high pressure phase above 5 kbar the temperature dependences of resistance becomes weak. Under the pressure above 7 kbar, the resistance is nearly constant. In this situation, the hole density depends strongly on temperature as shown in Fig. 8. At 18 kbar, for example, it changes by about five orders of magnitude from 300 to 1.5 K. The hole mobility, on the other hand, increases with decreasing temperature. Here again, we find an example in which the changes in the carrier density and the mobility occur in such a way that the resistance remains constant.

The temperature dependence of the carrier density suggests that θ-(BEDT-TTF)$_2$I$_3$ under hydrostatic pressures above 5 kbar is an ultra narrow gap semiconductor. Between 10 and 50 K, the carrier density depends on temperature as $n_{eff} \propto T^2$. Below 10 K, on the other hand, it obeys exponential law. The energy gap is estimated to be less than 0.5 meV.[35]

2.3.2 α-(BEDT-TSF)$_2$I$_3$

BEDT-TSF is a derivative of BEDT-TTF in which the four inner S-atoms in the BEDT-TTF molecule are replaced by Se-atoms. The crystal structure of α-(BEDT-TSF)$_2$I$_3$ resemble to that of α-(BEDT-TTF)$_2$I$_3$ (Fig. 1).[42] It is metallic above about 50 K where it changes to an insulator. When the pressure above 6 kbar is applied, insulating behavior at low temperature disappears and the conductivity is almost constant over the whole temperature region. Once again, we find the effect of which the cancellation between the strong temperature dependent hole density and the mobility gives the constant conductivity as shown in Fig. 8.

Above 20 K, the behavior of carriers is qualitatively the same with other two materials. Below 20 K, however, the behavior of the carrier system is different. The carrier density of other two materials is still changing at low temperatures such as 2 K. In α-(BEDT-TSF)$_2$I$_3$, on the other hand, below 20 K, the hole density saturates to a value of about 10^{17} cm^{-3}. This indicates this sample is not a semiconductor but a semimetal.

An important fact is that the carrier mobility is also constant below 20 K. The change of the density and mobility looks to be correlated. This fact suggests that the mechanism which determines the temperature dependence of the carrier density and the mobility is identical.

3. Phase Diagram of Uniaxially Compressed α-(BEDT-TTF)$_2$I$_3$

In the previous sections, α-(BEDT-TSF)$_2$I$_3$ under hydrostatic pressures were discussed. In this section, we mention the transport phenomena of this material when it is uniaxially compressed. The uniaxial strain method was developed by Maesato *et al.* They applied this technique to the α-(BEDT-TTF)$_2$I$_3$ and found that it behaves differently when compressed along different crystal axes.[3] Following this work, a more detailed experiment was done by Tajima *et al.*[5]

In this section, we describe the transport phenomena of α-(BEDT-TTF)$_2$I$_3$ under uniaxial strain along *a*- and *b*-axes. When the sample was compressed along *a*-axis, the superconducting state was discovered between charge ordered insulator phase and narrow gap semiconductor phase. When compressed along *b*-axis, on the other hand, this material changes to a two dimensional metal with a large Fermi surface.

3.1 *a-axis strain*

The temperature dependence of the resistance of samples under several uniaxial strains along the *a*-axis (p_a) is shown in Fig. 9. The metal–insulator transition is suppressed by this compression. When the strain is sufficiently large, we observe temperature-independent resistance (refer to the data for $p_a = 10$ kbar in Fig. 9) similar to that under high hydrostatic pressure. The temperature dependence of the mobility and the density of carriers was examined. Both of them depend strongly on temperature. They change by about three orders of magnitude from 70 to 1.5 K in such a manner that their temperature dependences cancel out with each other to give the temperature independent conductivity. At the lowest temperature, the system is in the state with

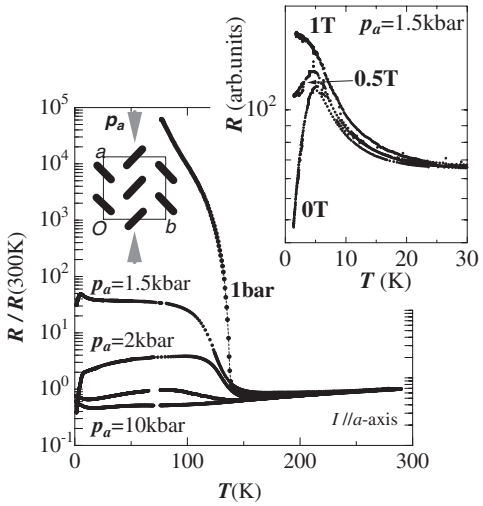

Fig. 9. Temperature dependence of the resistance when the sample is strained along the *a*-axis. The upper panel shows the effect of magnetic field on the resistance for the sample under the strain of $p_a = 1.5$ kbar.

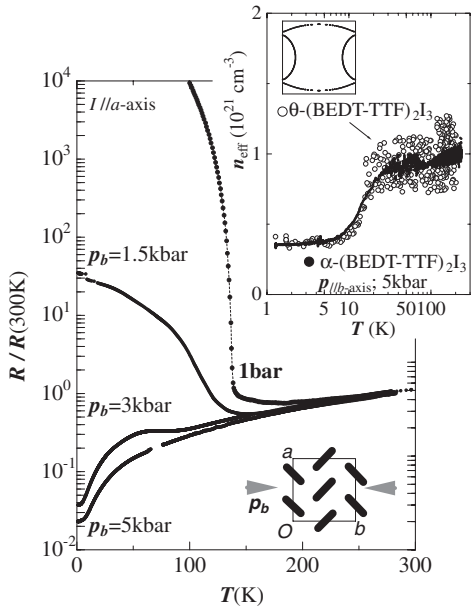

Fig. 10. Temperature dependence of resistance under strain along the *b*-axis. The upper panel shows the temperature dependence of the effective carrier density for the sample under a strain of $p_b = 5$ kbar. The data of θ-(BEDT-TTF)$_2$I$_3$ (open circles) are also plotted for comparison. The picture at the top of the figure in upper panel is a schematic drawing of the Fermi surface of θ-(BEDT-TTF)$_2$I$_3$.

low density ($n \sim 10^{16}$ cm^{-3}) and high mobility [$\mu \sim 10^5$ cm^2/(V·s)].[5)]

These observations tell that this material under high strain along *a*-axis is an ultra narrow gap semiconductor. The energy gap is estimated to be less than 5 meV. The carrier density obeys $n_{\mathrm{eff}} \propto T^2$ in the region from 10 to 50 K. Below 10 K, on the other hand, it decreases with exponential law.

Another important phenomenon we notice in Fig. 9 is abrupt drops in the resistance seen at the lowest temperatures in the sample under intermediate strains. A drop in the resistance below 5 K is recognized in the data of $p_a = 1.5$ kbar. In the sample under $p_a = 2$ kbar, the anomaly apparently shifts to a higher temperature (7.2 K). This drop is also recognized in the data for $p_a = 3$ kbar. When the sample is strongly strained (for example $p_a = 10$ kbar), the drop disappears. This anomaly is sensitive to magnetic fields as demonstrated in the inset of Fig. 9. The field of 1 T fully destroys the anomaly. Based on these observations this anomaly was ascribed to the appearance of the superconducting state.

This superconducting state is interesting because the density of carriers estimated from the Hall coefficient is quite low. How the superconducting state is formed. A clue to answer this question is obtained in the experimental results of magnetoresistance. It suggests the existence of an energy band with very high density of states, located close to the Fermi energy as discussed in §4.[18,19)] According to the theoretical work by Kobayashi *et al.*, the superconductivity is caused by the spin fluctuation associated with the large density of state near the Fermi level such as shown in Fig. 7.[36)]

3.2 b-axis strain

When the crystal is uniaxially compressed along the *b*-axis, the sample exhibits different transport phenomena. Under the compression along the *a*-axis, the resistance almost independent of temperature is observed as shown in Figs. 3 and 9. When compressed along the *b*-axis, in contrast, the sample shows the resistance that decreases by about two orders of magnitude from 300 to 4 K (the data for $p \parallel b = 5$ kbar in Fig. 10). It suggests that the metallic state is stabilized by the uniaxial strain along the *b*-axis.[3,5)]

Additional information was obtained from the Hall effect measurements. The carrier density (n_{eff}) estimated from the Hall coefficient remains high in all the temperature region (inset of Fig. 10). The temperature dependence of carrier density resembles that of θ-(BEDT-TTF)$_2$I$_3$ under ambient pressure.[35)] The coincidence is not only qualitative but also quantitative including a drop in the carrier density that occurs between 30 and 10 K. Therefore, α-(BEDT-TTF)$_2$I$_3$ compressed along the *b*-axis is considered to be a two-dimensional metal having a band structure very similar to that of θ-(BEDT-TTF)$_2$I$_3$.

In conclusion, an organic conductor α-(BEDT-TTF)$_2$I$_3$ exhibits different transport phenomena when it is strained in the *a*-direction and in the *b*-direction. They are summarized in schematic diagrams in Fig. 11.[5)]

4. Electron System in Magnetic Field

One of the characteristic property of an ultra narrow gap semiconductor is that the carrier system has extremely low density and high mobility in the lowest temperature region (Fig. 5). Such a highly mobile carrier system is supposed to be sensitive to the magnetic field.

The magneto-transport phenomena of α-(BEDT-TTF)$_2$I$_3$ were first investigated by Ojiro *et al.* They discovered anomalously large magnetoresistance and buildup of a large Hall voltage at low temperatures when the magnetic field is applied normal to the two-dimensional plane.[16,17)]

In this section, we discuss the carrier states of α-(BEDT-TTF)$_2$I$_3$ in the magnetic field.

Figure 12 shows the temperature dependence of the resistance in some magnetic fields up to 15 T at 18 kbar.[18,19)] In the absence of the magnetic field, the resistance decreases

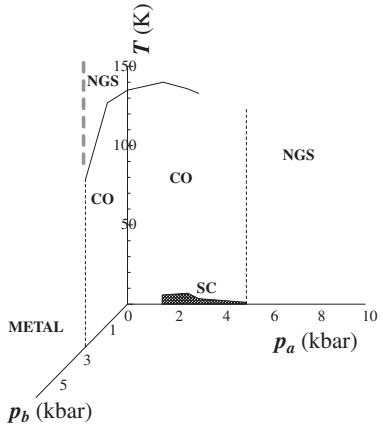

Fig. 11. Tentative phase diagram of α-(BEDT-TTF)$_2$I$_3$ under the strains (1) along the *a*-axis (p_a) and (2) along the *b*-axis (p_b). Where, the "CO" and the "NGS" in the phase diagram are the charge-ordering states and narrow gap semiconducting states, respectively. Superconducting states are represented by "SC". (1) Note that the charge-ordered state does not necessarily mean the insulating state. As we see in Fig. 11, under strains, the system seems to have a finite conductivity at the lowest temperature limit. (2) Although we drew a boundary between the narrow gap semiconductor and metal, these two states cannot be distinguished in the high temperature regions.

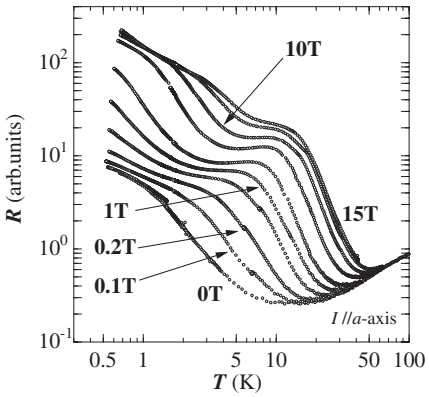

Fig. 12. Temperature dependence of the resistance under the magnetic field up to 15 T.

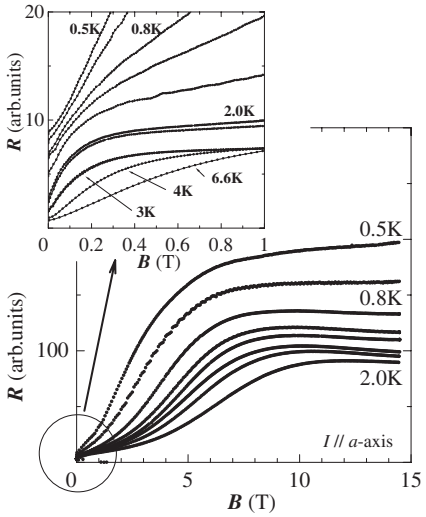

Fig. 13. Magnetic field dependence of the resistance down to 0.5 K. We show the low field region below 1 T in the inset.

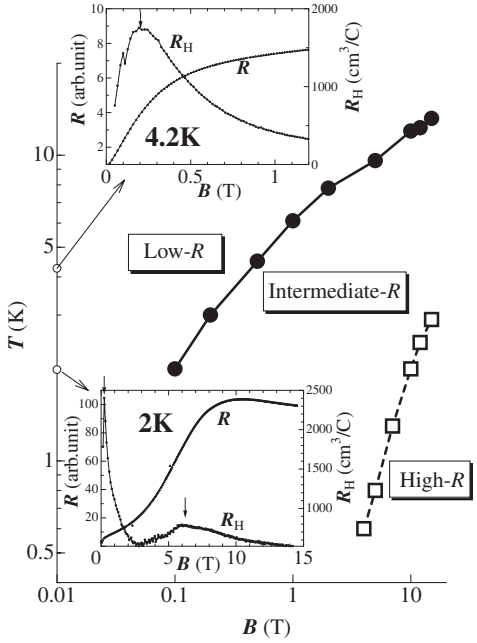

Fig. 14. Schematic diagram of boundaries between low-*R*, intemediate-*R* and high-*R* states in the *B*–*T* plane. Inset is the magnetic field dependence of the Hall coefficient and the resistance at 4.2 and 2 K.

with decreasing temperature down to 10 K, where it turns to increase. In a magnetic field, the resistance begins to increase at higher temperature. Following this rise, there appears a shoulder and then a step like flat region. At 1 T, for example, the shoulder locates at about 6 K. When the magnetic field is high, another shoulder appears at lower temperatures. In the curve for 10 T, for example, the first shoulder is seen at 15 K and the second shoulder around 2 K.

In Fig. 13, the resistance is plotted as functions of magnetic field with the temperature fixed.[18,19] Two step structure is clearly recognized. At 2 K, for example, a resistance rises in magnetic fields below 0.1 T and the successive saturation are observed (upper panel of the figure). The round off of the curve around 0.2 T makes the first shoulder. The grow up of the curve starts again at the field around 3 to 4 T and then the second shoulder appears at the field 8 to 10 T (main panel).

These experimental data suggest that with increasing magnetic field or decreasing temperature, the system changes from the low resistance (low-*R*) state to the intermediate-*R* state and then to the high-*R* state. Using the data in Figs. 12 and 13, we depict the boundaries between those state in the *B*–*T* plane in Fig. 14. In the transition region from low-*R* state to intermediate-*R* state, a rise of the resistance and a peak in the Hall coefficient is observed.[18,19] For example, the data at 4.2 and 2 K is shown in inset of Fig. 14. A similar peak in the Hall coefficient was found to appear also in the transition region between the intermediate and high-*R* states.

A naive interpretation of the phenomena described above is to assume that near the Fermi energy, there exist three different types of carriers and the transport phenomena reflect the character of carriers giving the dominant contribution to the transport.

From the data of the Hall coefficient and the magneto-resistance, rough values of carrier density and mobility for the three states can be estimated.[18,19] The results are summarized as follows: The low-R region is characterized by carriers with extremely low density (about $10^{15}\,\mathrm{cm}^{-3}$) and high mobility [about $10^5\,\mathrm{cm}^2/(\mathrm{V\cdot s})$] as mentioned in the previous section. In the intermediate-R state, on the other hand, the carrier density is about one order of magnitude higher and the mobility is by about two orders of magnitude lower than those in low-R state. From the intermediate region to the high-R region, the carrier density increases by about one order and mobility decreases by about two orders of magnitude.

The transport phenomena in the low-R state can be ascribed to the carrier system related to the Dirac cone as mentioned above.[5] The origin of other two electron systems, on the other hand, is not clear now. Judging from the experimental results indicating that the mobility is low, they will have much heavier mass than that of carriers on the Dirac cone.

Similar phenomena are observed in other three materials θ-(BEDT-TTF)$_2$I$_3$ ($p > 5$ kbar), α-(BEDT-TSF)$_2$I$_3$ ($p > 6$ kbar) and α-(BEDT-STF)$_2$I$_3$ ($p > 18$ kbar).

5. Photo-Induced Insulator–Metal Transition

Recently, α-(BEDT-TTF)$_2$I$_3$ under the ambient pressure was found to exhibit photo-switching between the charge ordered insulating state and the metallic state.[20]

In this experiment, a pulsed laser with the polarization along the b-axis and with a wave vector perpendicular to the two dimensional plane was applied on the sample. Photo-pulse with the photon energy of about 2.7 eV (450 nm) and the pulse duration of about 5 ns was used. The pulsed voltage up to 20 V (670 V/cm) was applied between electrodes which is separated by 0.3 mm and arranged so that electric field along the a-axis is formed. The time sequence of the laser pulse and the voltage pulse is shown in Fig. 15(a).

Figure 15(b) shows the time evolution of the photocurrent after the Laser irradiation (the intensity of about $2\,\mathrm{MW/cm}^2$, b-axis polarization). Large photocurrent with two components is observed. The first component has a life time of about 120 ns. About 0.7 μs after the irradiation, the second component of the photocurrent starts to grow. This photocurrent does not decay with time, but keeps growing as long as the electric field is applied. At the peak position of the first component of the photocurrent, the resistivity of the sample was estimated to be less than $0.36\,\Omega\cdot$cm. It is by about 7 orders of magnitude less than the dark resistance of the sample ($\sim 4\,\mathrm{M}\Omega\cdot$cm) at this temperature. For the second component, the photocurrent grows as time elapses, and therefore the resistance decreases with time. After 80 μs of irradiation, the resistivity becomes less than $0.4\,\Omega\cdot$cm. These values are comparable to that in the metallic state of this material under a high pressure. In conclusion, after irradiating Laser pulse with the b-polarization, two photo-induced metallic states appears successively. Hereafter, we call them the first conducting state and the second conducting state.

5.1 *First conducting state*

First, we discuss the first conducting state. This state appears when the laser pulse is irradiated with intensity above the threshold value. The threshold intensity is about $0.01\,\mathrm{MW/cm}^2$ for the Laser light of the wave length 450 nm (2.7 eV) at 4.2 K. The photocurrent depends non-linearly on Laser pulse intensity. On the other hand, it is proportional to the applied electric field.

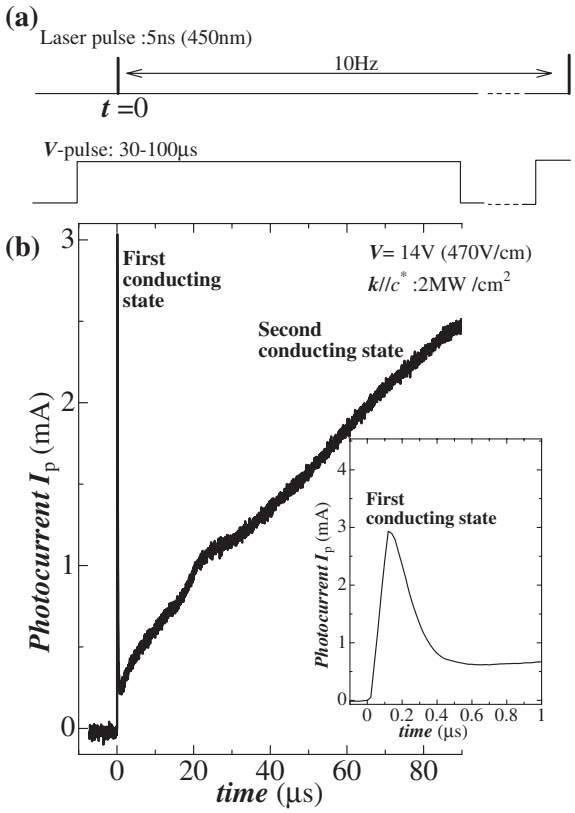

Fig. 15. (a) The timing of laser pulse (photon energy of 2.7 eV) and electric field pulse. (b) Time evolution of photocurrent for α-(BEDT-TTF)$_2$I$_3$ at 4 K. The laser power for the b-axis polarization is about $2\,\mathrm{MW/cm}^2$ and the electric field is 470 V/cm. The region up to 1 μs is expanded in the inset.

The wave length dependence of photocurrent in the first conducting state has its maximum at 450 nm. This energy of 2.7 eV is close to the intra-molecular HOMO–LUMO gap of neutral BEDT-TTF molecules. Therefore, the appearance of the first conducting state is expected to be associated with the intra-molecular excitation in BEDT-TTF molecules. The conductivity in this first conducting sate is strongly anisotropic. The ratio of the conductivity between a- and b-axes σ_b/σ_a is larger than 5.

5.2 *Second conducting state*

The second conducting state appears when the strong Laser light is shed on the sample on which strong electric field is applied. Under a low laser power or low electric field, the photocurrent decays rapidly toward zero and the system returns to the charge ordered insulating state. The threshold power of irradiation is $1.4-2.0\,\mathrm{MW/cm}^2$, and the threshold electric field is 470 V/cm. The photocurrent in the second conducting state exhibits highly nonlinear responses both to the laser power and to the electric field.

Similar photoconduction phenomena were discovered for the charge ordered state of the perovskite manganite $Pr_{0.7}Ca_{0.3}MnO_3$ by Miyano *et al.*[43]

Important information is that the second conducting state is not observed when the electric field is applied along *b*-axis. Note that in this direction, stripe pattern in the charge ordered state extends (Fig. 3). This suggests that the appearance of the second conducting state is associated with the stripe pattern of the charge ordered state. In this sense, the second conducting state is different from the first conducting state.

In conclusion, photo-induced insulator–metal transition was discovered in charge ordered insulating state of α-(BEDT-TTF)$_2$I$_3$ at low temperatures. Two metallic states (the first and second conducting states) were induced by irradiating Laser pulse with the *b*-axis polarization and with the photon energy about 2.7 eV. In the metallic phases (first and second conducting states), the resistivity is about $1/10^7$ of that without irradiation. The first conducting state disappears within about 120 ns. The second conducting state, on the other hand, appears as long as the high electric field along *a*-axis is applied.

6. Conclusions

In this paper, we described various types of transport phenomena that α-(BEDT-TTF)$_2$I$_3$ exhibits when the sample is placed under the (1) hydrostatic pressure, or (2) uniaxially compressed, or when (3) magnetic fields are applied, or irradiated by (4) strong light.

The experiments so far done indicate that; (1) α-(BEDT-TTF)$_2$I$_3$ under the high hydrostatic pressure is a new type of narrow gap (or zero gap) semiconductor. The carrier density and the mobility depend strongly on temperature. They change by about six orders of magnitude from 300 to 1.5 K. Below 50 K, the temperature dependence of the carrier density obey $n \propto T^2$. (2) Uniaxially compressed samples exhibit several phases of transport phenomena; Depending on the direction of the compression, the system changes from the charge ordered insulating phase to a narrow gap semiconductor or to a metal. Superconducting state was discovered in the sample which is uniaxially compressed along *a*-axis. (3) Transport phenomena of α-(BEDT-TTF)$_2$I$_3$ under high hydrostatic pressures are very sensitive to the magnetic field at low temperatures. Two steps of change in the carrier system was observed in the magnetic fields. It is interpreted in terms of three groups of carriers which are assumed to exist near the Fermi energy level. (4) Photo-switching between a charge-ordered insulating state and a metallic state was realized when the light with the photon energy of about 2.7 eV was irradiated on α-(BEDT-TTF)$_2$I$_3$ under ambient pressure at low temperatures.

Acknowledgements

We are grateful to R. Kato, T. Naito, J. Fujisawa, N. Naka, T. Ishihara and Y. Iye for fruitful collaborations which helped us understand the subjects discussed in this paper. This work is partially supported by a Grant-in-Aid for Scientific Research on Priority Areas of Molecular Conductors (No. 15073222) from the Ministry of Education, Culture, Sports, Science and Technology, Japan.

1) T. Ishiguro and K. Yamaji: *Organic Superconductors* (Springer-Verlag, Berlin, 1990).
2) H. Taniguchi, M. Miyashita, K. Uchiyama, K. Satoh, N. Mori, H. Okamoto, K. Miyagawa, K. Kanoda, M. Hedo and Y. Uwatoko: J. Phys. Soc. Jpn. **74** (2003) 468.
3) M. Maesato, Y. Kaga, R. Kondo and S. Kagoshima: Rev. Sci. Instrum. **71** (2000) 176.
4) N. Tajima, M. Tamura, Y. Nishio, K. Kajita and Y. Iye: J. Phys. Soc. Jpn. **69** (2000) 543.
5) N. Tajima, A. Ebina-Tajima, M. Tamura, Y. Nishio and K. Kajita: J. Phys. Soc. Jpn. **71** (2002) 1832.
6) S. Tomić, J. R. Cooper, D. Jérome and K. Bechgaard: Phys. Rev. Lett. **62** (1989) 462.
7) K. Inagaki, I. Terasaki, H. Mori and T. Mori: J. Phys. Soc. Jpn. **73** (2004) 3364.
8) S. Uji, H. Shinagawa, T. Terashima, T. Yakabe, Y. Terai, M. Tokumoto, A. Kobayashi, H. Tanaka and H. Kobayashi: Nature **410** (2001) 908.
9) T. Takahashi, D. Jérome and K. Bechgaard: J. Phys. Lett. (Paris) **51** (1982) L565.
10) D. Andres, M. V. Kartsovnik, P. D. Grigoriev and H. Müller: Phys. Rev. B **68** (2003) 201101(R).
11) F. O. Karutz, J. U. von Schütz, H. Wachtel and H. C. Wolf: Phys. Rev. Lett. **81** (1998) 140.
12) M. Chollet, L. Guerin, N. Uchida, S. Fukaya, H. Shimoda, T. Ishikawa, K. Matsuda, T. Hasegawa, A. Ota, H. Yamochi, G. Saito, R. Tazaki, S. Adachi and S. Koshihara: Science **307** (2005) 86.
13) T. Mishima, T. Ojiro, K. Kajita, Y. Nishio and Y. Iye: Synth. Met. **69–71** (1995) 771.
14) N. Tajima, M. Tamura, Y. Nishio, K. Kajita and Y. Iye: J. Phys. Soc. Jpn. **69** (2000) 543.
15) N. Tajima, A. Ebina-Tajima, M. Tamura, Y. Nishio and K. Kajita: J. Phys. Soc. Jpn. **71** (2002) 1832.
16) T. Ojiro, K. Kajita, Y. Nishio, H. Kobayashi, A. Kobayashi, R. Kato and Y. Iye: Synth. Met. **55–57** (1993) 2268.
17) K. Kajita, T. Ojiro, H. Fujii, Y. Nishio, H. Kobayashi, A. Kobayashi and R. Kato: J. Phys. Soc. Jpn. **61** (1993) 23.
18) N. Tajima, M. Tamura, Y. Nishio, K. Kajita and Y. Iye: Synth. Met. **103** (1999) 1960.
19) K. Kajita, N. Tajima, M. Tamura and Y. Nishio: 4th Int. Symp. Advanced Physical Fields "Quantum Phenomena in Advanced Materials at High Magetic Fiels", 1999, p. 79.
20) N. Tajima, J. Fujisawa, N. Naka, T. Ishihara, R. Kato, Y. Nishio and K. Kajita: J. Phys. Soc. Jpn. **74** (2005) 511.
21) K. Bender, I. Hennig, D. Schweitzer, K. Dietz, H. Endres and H. J. Keller: Mol. Cryst. Liq. Cryst. **108** (1984) 359.
22) R. P. Shibaeva, V. F. Kaminskii and E. B. Yagubskii: Mol. Cryst. Liq. Cryst. **119** (1985) 361.
23) H. Kobayashi, R. Kato, A. Kobayashi, Y. Nishio, K. Kajita and W. Sasaki: Chem. Lett. (1986) 833.
24) H. Kobayashi, R. Kato, A. Kobayashi, Y. Nishio, K. Kajita and W. Sasaki: Chem. Lett. (1986) 789.
25) A. Kobayashi and H. Kobayashi: to be published.
26) B. Rothaemel, L. Forró, J. R. Cooper, J. S. Schilling, M. Weger, P. Bele, H. Brunner, D. Schweitzer and H. J. Keller: Phys. Rev. B **34** (1986) 704.
27) H. Kino and H. Fukuyama: J. Phys. Soc. Jpn. **64** (1995) 1877.
28) H. Seo: J. Phys. Soc. Jpn. **69** (2000) 805.
29) Y. Takano, K. Hiraki, H. M. Yamamoto, T. Nakamura and T. Takahashi: J. Phys. Chem. Solids **62** (2001) 393.
30) R. Wojciechowski, K. Yamamoto, K. Yakushi, M. Inokuchi and A. Kawamoto: Phys. Rev. B **67** (2003) 224105.
31) M. V. Kartsovnik, P. A. Kononvich, V. N. Laukin, A. G. Khomenko and I. F. Schegolev: Sov. Phys. JETP **61** (1985) 866.
32) H. Schwenk, F. Gross, C. P. Heidmann, K. Andres, D. Schweitzer and H. Keller: Mol. Cryst. Liq. Cryst. **119** (1985) 329.
33) N. Tajima, A. Ebina, Y. Nishio and K. Kajita: 10th Int. Conf. Narrow Gap Semiconductors, 2001, p. 303.
34) M. T. Czyzyk and M. Podgorny: Phys. Status Solidi B **98** (1980) 507.
35) N. Tajima, A. Tajima, M. Tamura, R. Kato, Y. Nishio and K. Kajita: J. Phys. IV (Paris) **114** (2004) 263.
36) A. Kobayashi, S. Katayama, K. Noguchi and Y. Suzumura: J. Phys. Soc. Jpn. **73** (2004) 3135.
37) R. Kondo and S. Kagoshima: J. Phys. IV (Paris) **114** (2004) 523.
38) K. Kajita, Y. Nishio, T. Takahashi, W. Sasaki, R. Kato, H. Kobayashi, A. Kobayashi and Y. Iye: Solid State Commun. **70** (1989) 1189.

39) M. Tamura, H. Kuroda, S. Uji, H. Aoki, M. Tokumoto, A. G. Swanson, J. S. Brooks, C. C. Agosta and S. T. Hannahs: J. Phys. Soc. Jpn. **63** (1994) 615.
40) T. Terashima, S. Uji, H. Aoki, M. Tamura, M. Kinoshita and M. Tokumoto: Synth. Met. **70** (1995) 845.
41) M. Tamura, F. Matsunaga, N. Tajima, Y. Nishio and K. Kajita: Synth. Met. **86** (1997) 2007.
42) R. Kato, H. Kobayashi and A. Kobayashi: Synth. Met. **42** (1991) 2093.
43) K. Miyano, T. Tanaka, Y. Tomioka and Y. Tokura: Phys. Rev. Lett. **78** (1997) 4257.

Naoya Tajima was born in Kumamoto Prefecture, Japan in 1970. He obtained his Ph. D. (1999) degrees from Toho University. He was a research associate (1999–2001) at Faculty of Science, Gakushuin University and Ph. D. (2001–2003) at RIKEN. Since 2003 he has been a scientist at RIKEN. He has worked on organic conductors, particularly on transport properties. His main research is focused on searching for the new physics underling the ultra narrow (zero) gap organic semiconductors with Dirac-cone type energy dispersion.

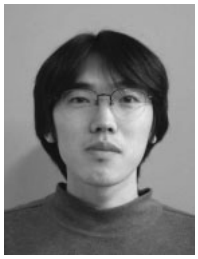

Shigeharu Sugawara was born in Chiba Prefecture, Japan in 1980. He obtained his B. Sc. (2003) and M. Sc. (2005) degrees from Toho University. His main interest is in the effect of magnetic field on the transport phenomena of organic layered metals or semiconductors.

Masafumi Tamura was born in Kyoto Prefecture, Japan in 1964. He obtained B. Sc. (1986), M. Sc. (1988), and D. Sc. (1995) degrees from the University of Tokyo. He was a research associate at the Institute for Solid State Physics, the University of Tokyo (1990–1995), a lecturer at Faculty of Science, Toho University (1995–2000), and a senior research scientist at RIKEN (2000–2001). Since 2001, he has been a senior scientist at RIKEN. He has worked on molecule-based conducting or magnetic materials, particularly on their magnetic or optical properties. His recent research is focused mainly on the chemical design and physical characterization of the molecular materials having degenerate ground states, such as frustrated spin systems.

Yutaka Nishio was born in Tottori Prefecture, Japan in 1954. He obtained his B. Sc. (1979), M. Sc. (1981), and D. Sc. (1984) degree from Tohoku University. He was a research associate (1984–1987), a lecturer (1987–1992), an associate professor (1992–2002) and a professor (2002–) at Faculty of Science, Toho University. He started his career as a physicist from the investigation of disorder induced metal–insulator transitions in layered compounds. Afterward, he expanded his work to doped semiconductors. Then, he moved to the investigation of organic materials. He is interested in thermal properties of organic conductors, especially in the vicinity of the phase transition such as that from metallic state to charge ordered insulating state.

Koji Kajita was born in Gifu, Japan in 1944. He received his B. Sc. (1967), M. Sc. (1969), and D. Sc. (1972) from the University of Tokyo. From 1973 to 1983, he was a research associate at Tokyo University. During this period, he worked in the field of ferro-magnetic semiconductors, hot electron effect of photo-excited electrons and two-dimensional electrons trapped on dielectric materials. In 1983, he moved to Toho University as an associate professor. Since 1988, he has been a professor. For this decade, he was engaged in the investigation of electrical transport phenomena in organic materials.